Supplementary Information

Projected changes in heatwaves over Central and South America using high-resolution regional climate simulations

Ramarao M.V.S.[1,11], Saravanan Arunachalam[1*], Brisa Sánchez[2], Leah H Schinasi[2], Maryia Bakhtsiyarava[3], Waleska Teixeira Caiaffa[4], Iryna Dronova[5], Marie S. O'Neill[6], Ione Avila-Palencia[7], Nelson Gouveia[8], Yang Ju[3,9], Josiah L. Kephart[10], Daniel A. Rodríguez[3]

1. Institute for the Environment, University of North Carolina at Chapel Hill, Chapel Hill, NC 27599, USA
2. Department of Epidemiology and Biostatistics, Dornsife School of Public Health, Drexel University, Philadelphia, PA, USA
3. Department of City and Regional Planning and Institute for Transportation Studies, University of California, Berkeley, CA, USA
4. Observatory for Urban Health in Belo Horizonte, Federal University of Minas Gerais, Av. Pres. Antônio Carlos, 6627 - Pampulha, Belo Horizonte, MG, 31270-901, Brazil.
5. Department of Environmental Science, Policy and Management and Department of Landscape Architecture and Environmental Planning, University of California Berkeley, Berkeley, CA, USA 94720
6. Department of Environmental Health Sciences, University of Michigan School of Public Health, Ann Arbor, USA
7. Centre for Public Health, School of Medicine, Dentistry and Biomedical Sciences, Queen's University Belfast, Belfast, Northern Ireland, United Kingdom
8. Department of Preventive Medicine, University of Sao Paulo Medical School, Sao Paulo, Brazil
9. School of Architecture and Urban Planning, Nanjing University, Nanjing, China
10. Urban Health Collaborative, Drexel Dornsife School of Public Health, Philadelphia, PA, USA
11. National Centre for Medium Range Weather Forecasting, MoES, Noida, UP-201309, India

∗ Author to whom any correspondence should be addressed.

E-mail: sarav@email.unc.edu

Supplementary Notes:

Details of WRF simulations

WRF is a nonhydrostatic mesoscale meteorological model widely used for regional weather and climate applications across the globe [1]. For this study, the 4.1.4 version of the WRF model was used to dynamically downscale the regional climate over Latin America with a spatial resolution of 12 km × 12 km. The WRF parameterization options used for this study include WRF single-moment 5-class micro physics scheme, new Tiedtke cumulus parameterization scheme, Rapid Radiative Transfer Model for GCMs (RRTMG) shortwave and longwave schemes [2], Yonsei University planetary boundary layer scheme [3], MM5 similarity surface layer scheme [4] and Noah land surface model [5].

For computational efficiency, entire Latin America land region is divided into two smaller domains: Central America (CAM, including Mexico) and South America (SAM). The WRF model was configured for each domain at 12 km × 12 km horizontal resolution with a time step of 60 seconds and 40 levels in the vertical. The number of grid points are 447 × 255 and 480 × 711 for CAM and SAM domains, respectively (Supplementary Figure 1). Three 11-year downscaling simulations were carried out using this model set-up for each domain, one for historical period (1995-2005; HIST) and two future simulations (2045-2054) following two extreme Intergovernmental Panel on Climate Change (IPCC) approved future scenarios namely Representative Concentration Pathway 2.6 (RCP 2.6) and 8.5 (RCP 8.5) to account for the full range of emission scenario uncertainty. RCP2.6 is a mitigation scenario in which the net radiative forcing reaches 3.1 Wm^{-2} by mid-century but returns to 2.6 Wm^{-2} by 2100 whereas RCP8.5 is the most-aggressive emission scenario in which the net radiative forcing at the end of 2100 is 8.5 Wm^{-2}. Earlier research has also found that both historical and near term (through 2050) cumulative emissions under current policies match very well with RCP 8.5 compared to other RCPs [6]. Since the use of the RRTMG radiation scheme permits the modification of greenhouse gases (GHG) with time, we used time-varying greenhouse gas concentrations based on the observed values for the historical period and based on the corresponding scenario for the future projection period. GHG emissions thus varied in time and their effects are reflected in radiation calculations in our simulations [7].

Given the large computational cost, we limited our downscaling experiments for a single ESM for the past and two future emission scenarios each for an 11-year period, with the first year considered as spin-up and omitted in the analyses. The initial and lateral boundary conditions came from the r1i1p1 ensemble of the global model MPI from the CMIP5 archive and the lateral boundary conditions were updated at 6 hourly intervals at the boundaries of the model domain.

Selection of MPI-ESM-LR as driving model

The Coupled Model Intercomparison Project Phase 5 (CMIP5) provides a suite of climate simulations from about 56 climate models with varying complexities for the research community. Out of these models, the low-resolution version of Max-Planck-Institute Earth System Model (MPI-ESM-LR; referred as MPI) model has been selected to drive WRF high resolution simulations based on a thorough literature review. It is noted that the MPI model has been widely used to drive various regional models including WRF and downscale finer climate information in CORDEX North and South America projects [8]. The MPI model simulations have been used in many global and regional studies for assessing the current as well as future changes in characteristics of essential climate parameters and extreme events like heatwaves [9], droughts [10], precipitation characteristics [11–13], multi-scale precipitation variability over South America [14]. Yin et al (2013) have shown that the MPI model better captures large-scale precipitation patterns during DJF, MAM and SON seasons over tropical South America compared to the other selected CMIP5 models in the study. MPI model is also found to be one among the five best models that accurately reproduce the modes of tropical Pacific sea level pressure variability [12]. Further, the MPI model has been used to drive high resolution WRF climate simulations and studies have documented its advantages. Fonseca et al (2016) have used MPI to drive WRF model over Iberian Peninsula and reported that the general sign of trends in extreme temperature and precipitation is similar to that obtained by a simulation driven with ERA-Interim reanalysis despite few differences in the magnitudes. Marta-Almeida et al (2016) also highlight the capability of the MPI-ESM driven WRF in simulating the observed climate over Iberian Peninsula, similar to the ERA-Interim driven WRF simulation. Knist et al (2018)have also found MPI model useful in downscaling the climate over Europe at convective permitting scales with the WRF model. Another study by ref. [17] have attempted to evaluate the model performance and rank the CMIP5 GCMs based on the empirical probability distribution functions of precipitation and temperature climatology of the entire spectrum and for the upper (>95th percentile) and lower tails (<5th percentile) of the distribution. The results reveal that the MPI-ESM-LR consistently performs better and stood within top 5 ranks in simulating the probability distribution of temperature for the global average and, in particular, over the regions of our interest, i.e., Central America (CAM), Amazon (AMZ), Central South America (CSA) and Southern South America (SSA) [17]. Based on the above results and discussion, we selected MPI-ESM-LR as a driving model to WRF high resolution simulations. Further details of the MPI-ESM-LR can be obtained from https://view.es-doc.org/?renderMethod=name&type=cim.1.software.ModelComponent&name=MPI-ESM-LR&project=CMIP5.

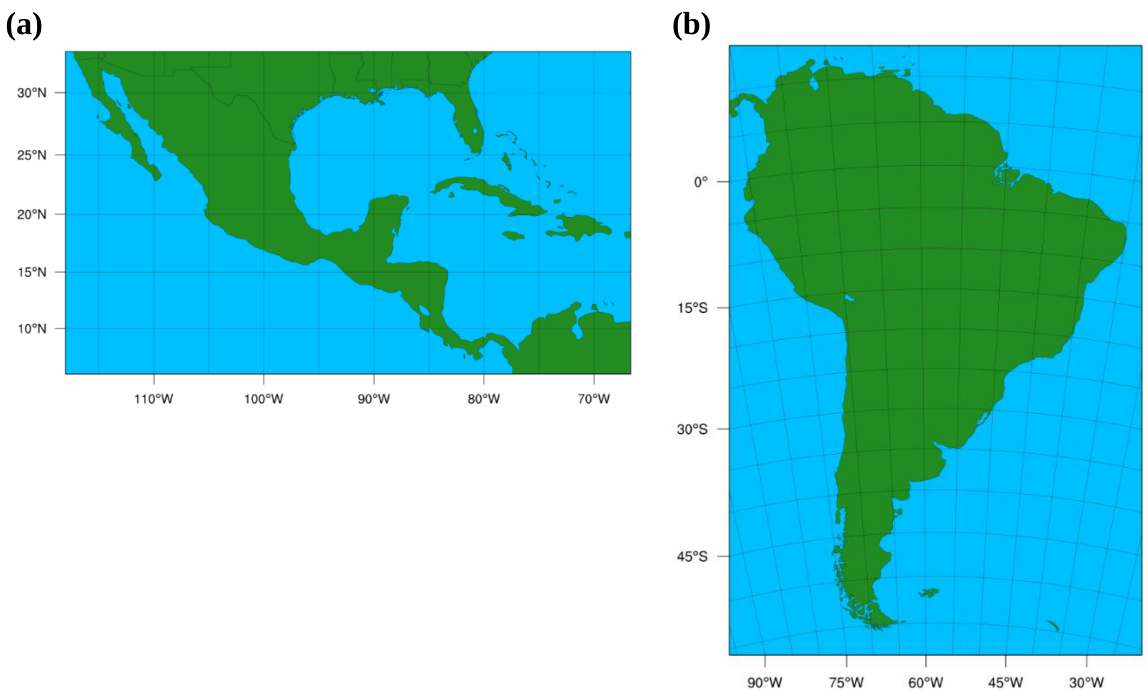

Supplementary Figure S1. Spatial domains used for WRF climate simulations (a) Central America (CAM) with 447 × 255 grid points and (b) South America (SAM) with 480 × 711 grid points at 12 km × 12 km horizontal resolution. This map was prepared using NCL (NCAR Command Language Version 6.4.0, https://www.ncl.ucar.edu/index.shtml).

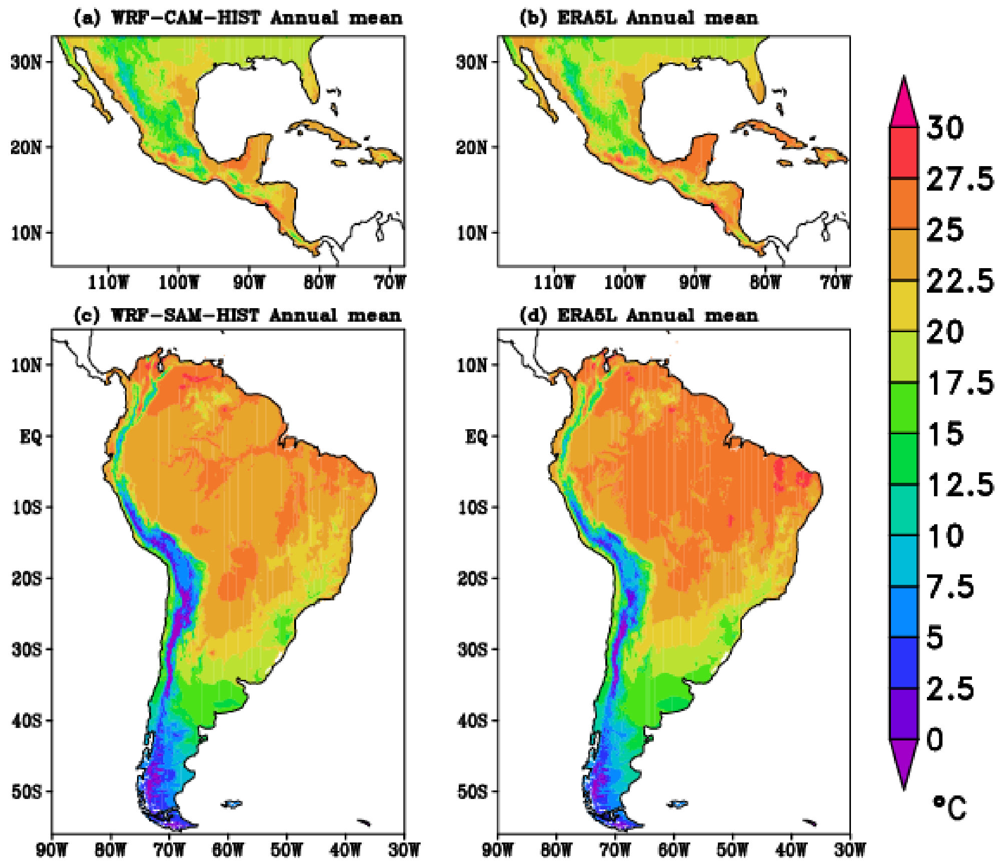

Supplementary Figure S2. Spatial distribution of Annual mean temperature. Annual mean temperature during the period 1996-2005 for (a,b) CAM and (c,d) SAM domains from (a,c)WRF simulation and (b,d) ERA5L data. (This map was generated using GrADS (Version 2.1.a3), https://cola.gmu.edu/grads/).

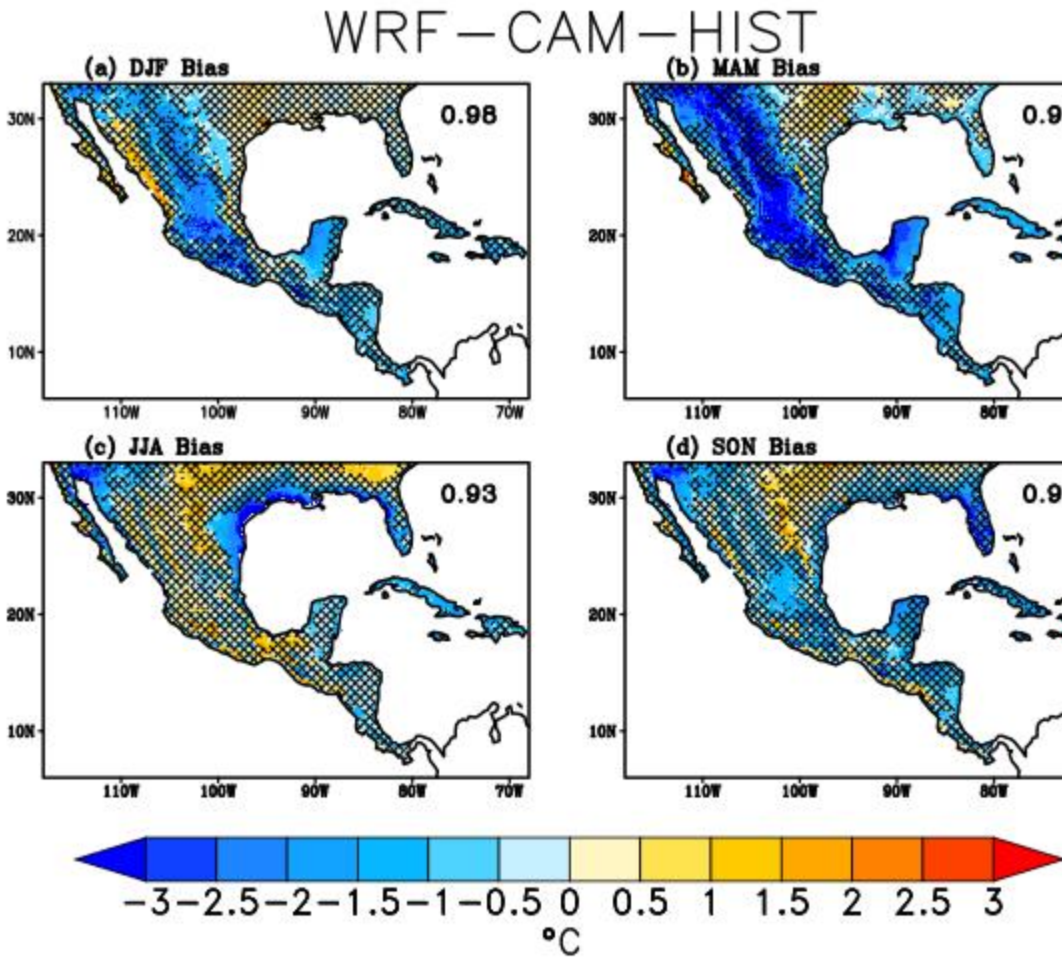

Supplementary Figure S3. Seasonal biases. Seasonal bias in daily mean temperature from WRF high resolution simulation for the CAM domain for (a) December-January-February (DJF), (b) March-April-May (MAM), (c) June-July-August (JJA) and (d) September-October-November (SON) seasons. Shading indicates the bias in temperature. Hatching indicates the grid points with value addition by WRF where the bias is lesser in WRF simulation than the driving GCM, MPI. Numerical values in each panel show the pattern correlation of respective seasonal mean temperature with ERA5L data. (This map was generated using GrADS (Version 2.1.a3), https://cola.gmu.edu/grads/).

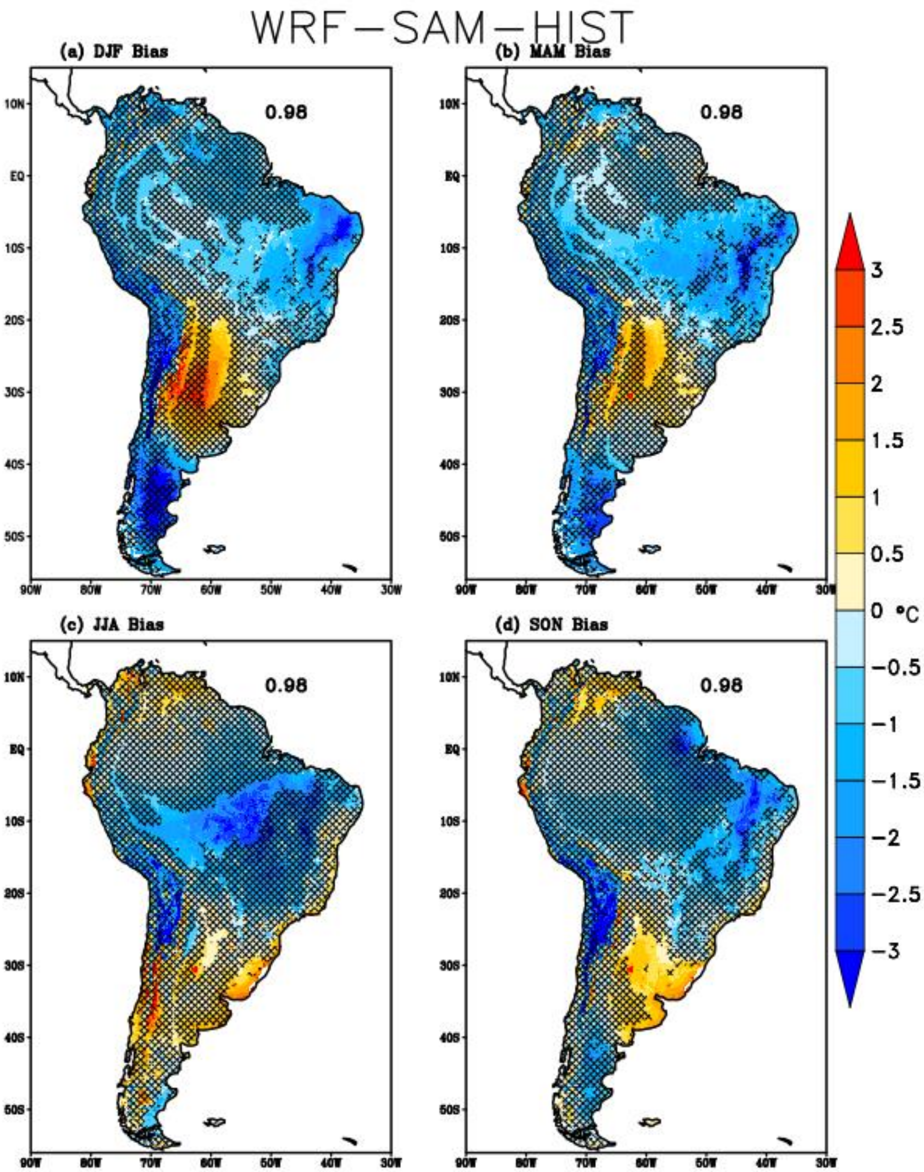

Supplementary Figure S4. Same as Supplementary Fig. S3, but for SAM domain. (This map was generated using GrADS (Version 2.1.a3), https://cola.gmu.edu/grads/).

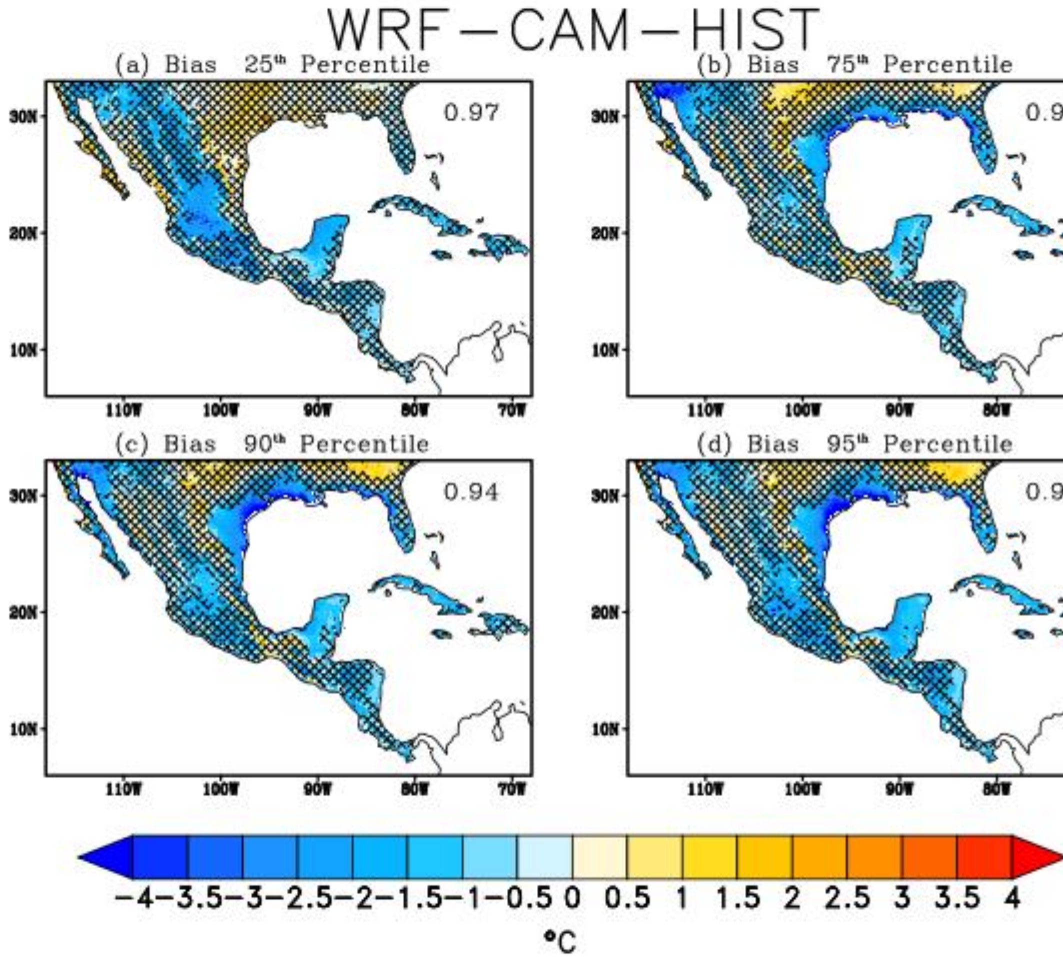

Supplementary Figure S5. Same as Supplementary Fig. S3, but for various percentile values of daily mean temperatures (a) 25th percentile (b) 75th percentile (c)90th percentile (d) 95th percentile. (This map was generated using GrADS (Version 2.1.a3), https://cola.gmu.edu/grads/).

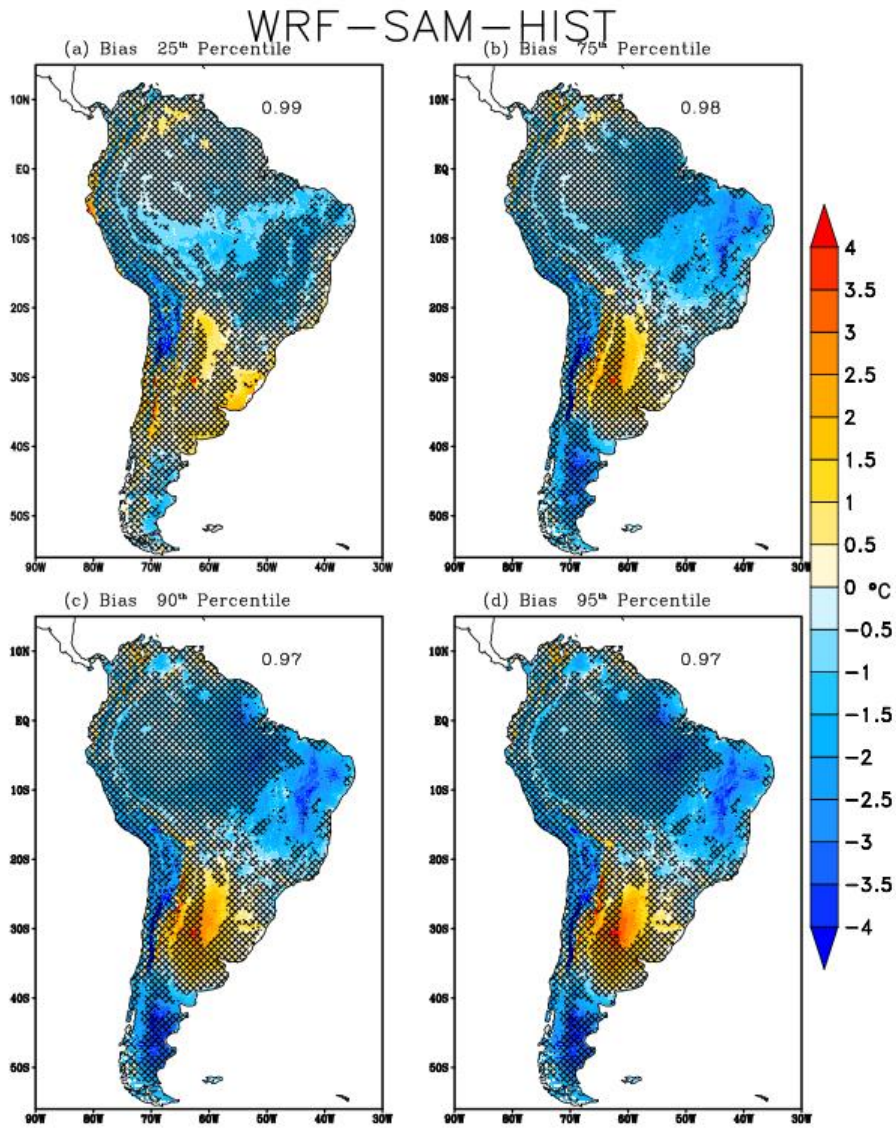

Supplementary Figure S6. Same as Supplementary Fig. S5, but for SAM domain. (This map was generated using GrADS (Version 2.1.a3), https://cola.gmu.edu/grads/).

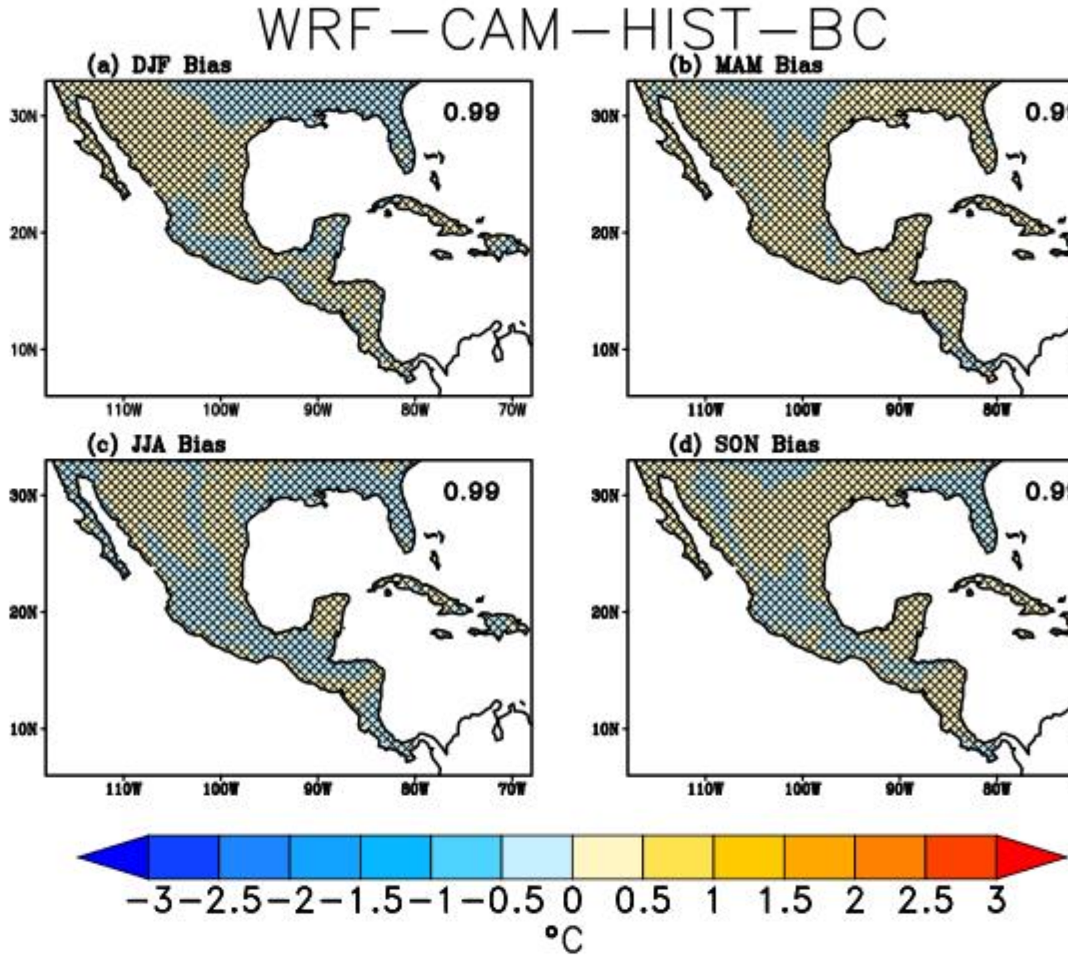

Supplementary Figure S7. Same as Supplementary Fig. S3, but for bias corrected WRF output. (This map was generated using GrADS (Version 2.1.a3), https://cola.gmu.edu/grads/).

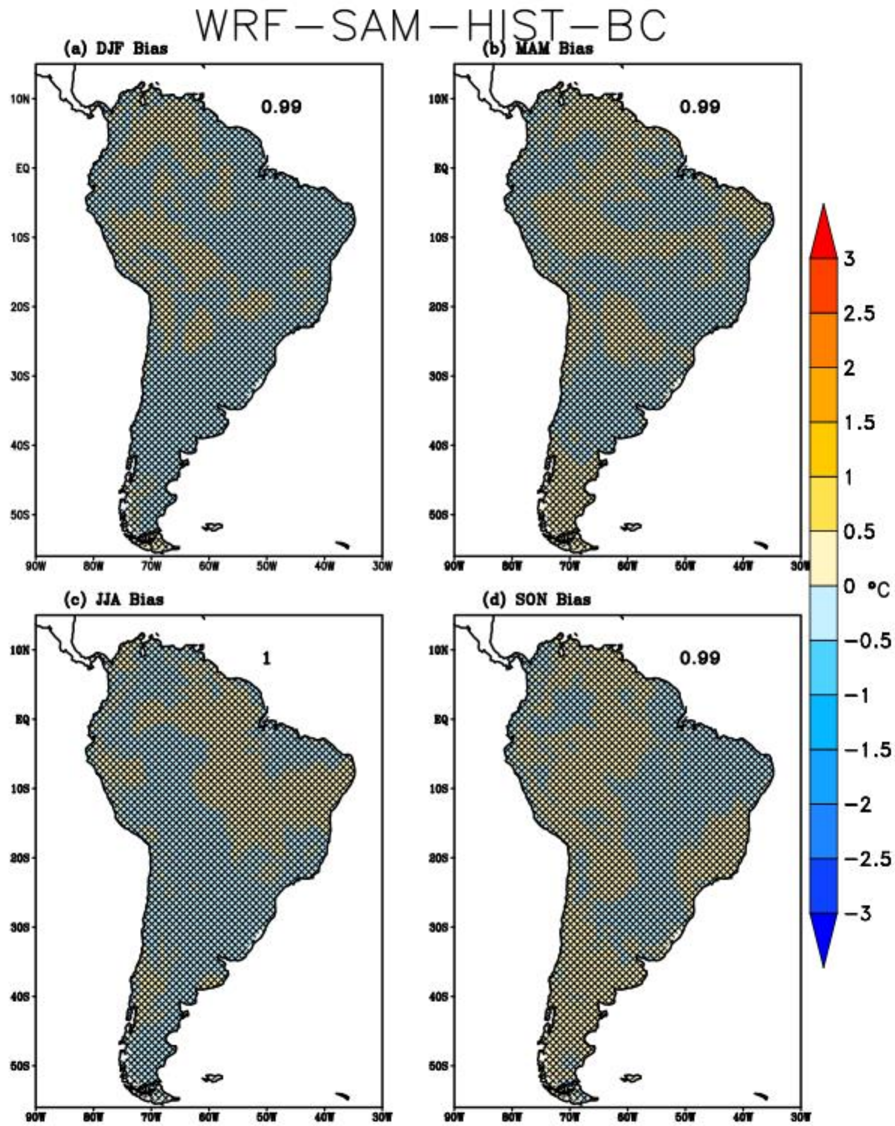

Supplementary Figure S8. Same as Supplementary Fig. S4, but for bias corrected WRF output. (This map was generated using GrADS (Version 2.1.a3), https://cola.gmu.edu/grads/).

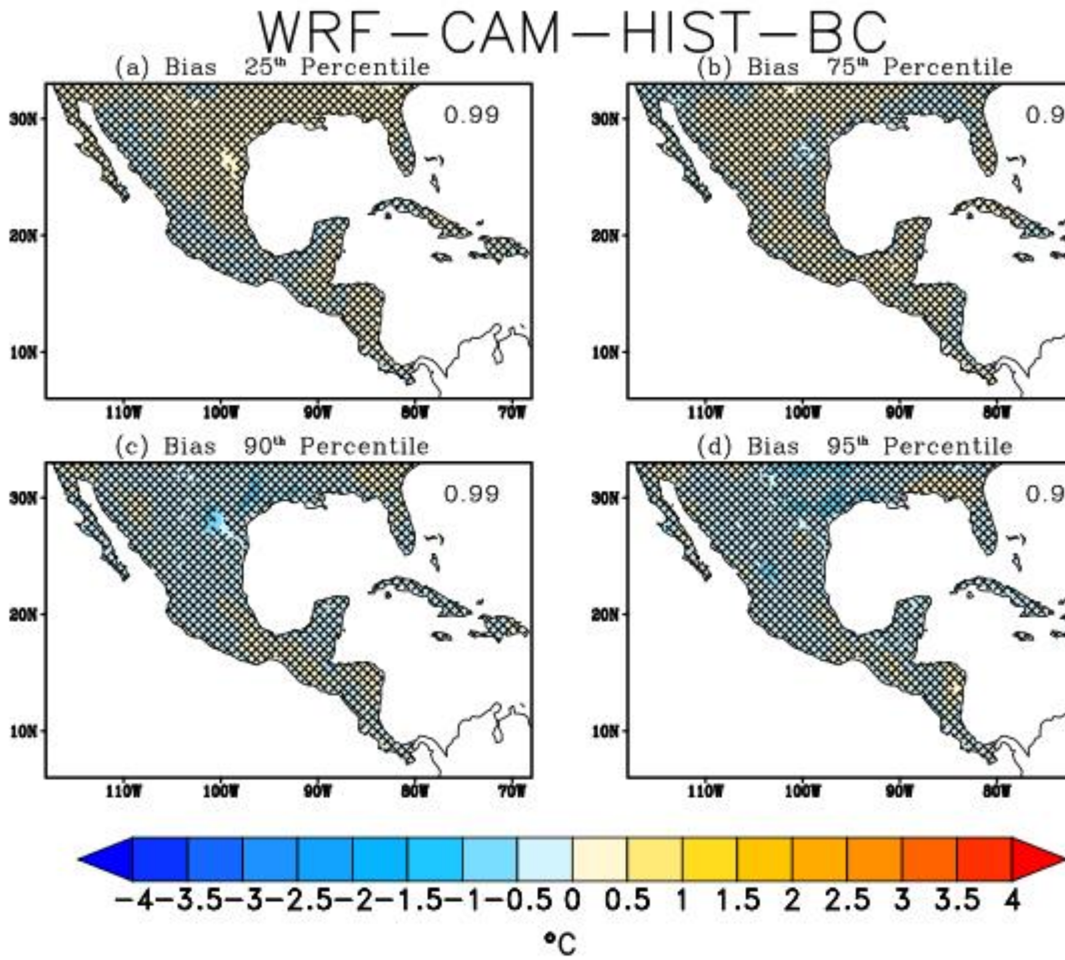

Supplementary Figure S9. Same as Supplementary Fig. S5, but for bias corrected WRF output. (This map was generated using GrADS (Version 2.1.a3), https://cola.gmu.edu/grads/).

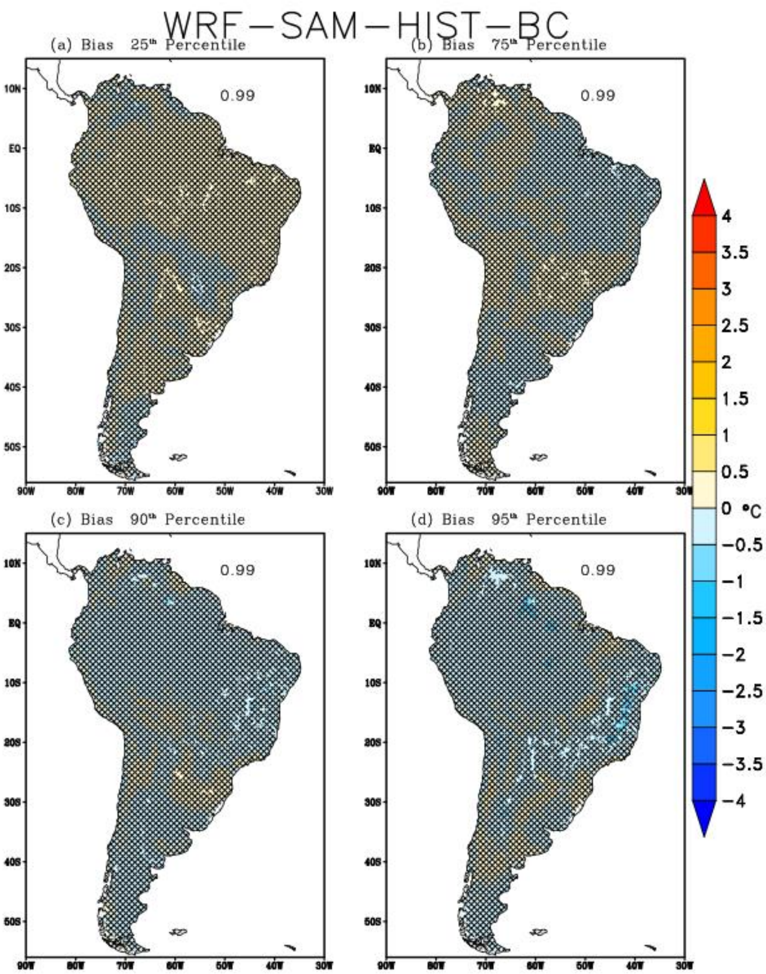

Supplementary Figure S10. Same as Supplementary Fig. S6, but for bias corrected WRF output. (This map was generated using GrADS (Version 2.1.a3), https://cola.gmu.edu/grads/).

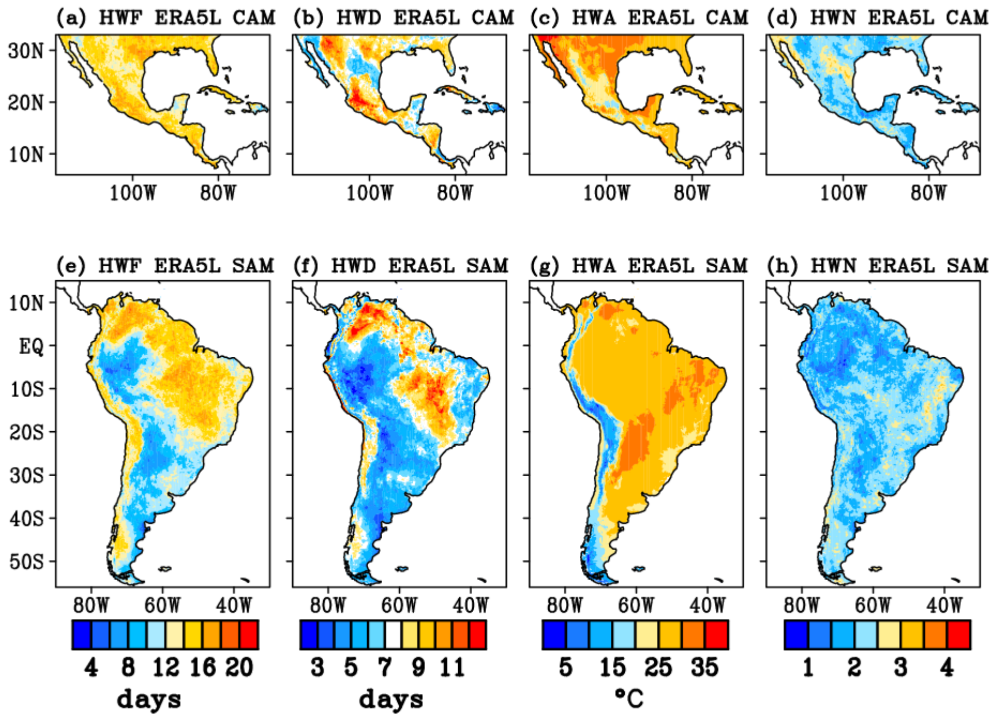

Supplementary Figure S11. Spatial distribution of HW metrics from ERA5L. Spatial distribution of HW metrics averaged for the base period 1996-2005 for (a-d) CAM and (e-h) SAM domains for (a, e) HWF; (b, f) HWD; (c, g) HWA and (d, h) HWN from ERA5L dataset. (This map was generated using GrADS (Version 2.1.a3), https://cola.gmu.edu/grads/).

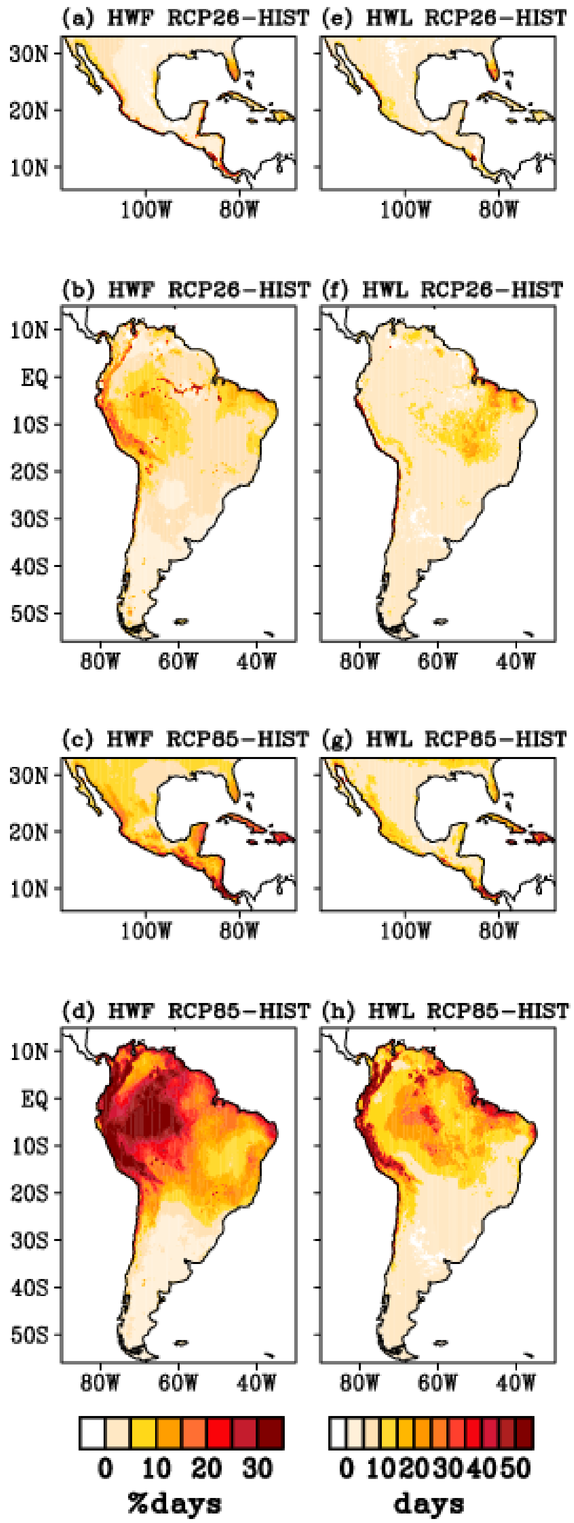

Supplementary Figure S12. Projected changes in HW metrics over the period 2045-2054 under (first and second rows) RCP2.6 and (third and fourth rows) RCP8.5 scenarios for (a-d) HWF as % of annual days; (e-h) HWL, the average duration of HW in a year. (This map was generated using GrADS (Version 2.1.a3), https://cola.gmu.edu/grads/).

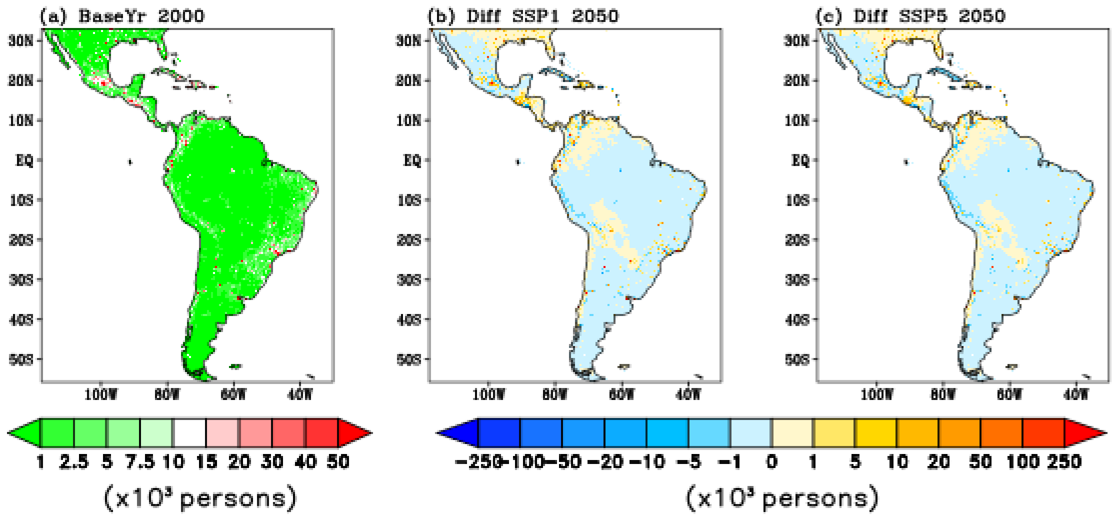

Supplementary Figure S13. Population counts. Spatial pattern of population counts over Latin America (a) for the base year 2000 and difference with base year for (b) the scenario SSP1 (c) the scenario SSP5 in the year 2050. (This map was generated using GrADS (Version 2.1.a3), https://cola.gmu.edu/grads/).

Supplementary Table S1. Comparison of area averaged HW metrics between the bias corrected WRF simulation and ERA5L data during the base period 1996-2005.

Sub-region	**HWF**			**HWD**			**HWA**			**HWN**		
	ERA5L	**WRF**	**Diff (WRF-ERA5)**	**ERA5L**	**WRF**	**Diff (WRF-ERA5)**	**ERA5L**	**WRF**	**Diff (WRF-ERA5)**	**ERA5L**	**WRF**	**Diff (WRF-ERA5)**
CAM	14.0	12.4	-1.6	8.0	6.0	-2.0	26.9	27.0	0.1	2.1	2.4	0.3
AMZ	12.9	11.0	-1.9	7.0	5.7	-1.3	26.7	26.6	-0.1	1.9	1.9	0
CSA	10.5	10.2	-0.3	5.8	5.5	-0.3	25.1	25.1	0	2.0	2.0	0
SSA	10.9	9.5	-1.4	6.0	5.1	-0.9	17.1	17.1	0	2.2	2.2	0
SAM	12.2	10.7	-1.5	6.6	5.6	-1.0	25.7	25.6	-0.1	1.9	2.0	0.1

Supplementary References

1. Skamarock, W. C. *et al.* A Description of the Advanced Research WRF Model Version 4.1. (2019) doi:10.5065/1DFH-6P97.

2. Iacono, M. J. *et al.* Radiative forcing by long-lived greenhouse gases: Calculations with the AER radiative transfer models. *Journal of Geophysical Research Atmospheres* **113**, (2008).

3. Hong, S. Y., Noh, Y. & Dudhia, J. A New Vertical Diffusion Package with an Explicit Treatment of Entrainment Processes. *Mon Weather Rev* **134**, 2318–2341 (2006).

4. Fairall, C. W., Bradley, E. F., Hare, J. E., Grachev, A. A. & Edson, J. B. Bulk Parameterization of Air–Sea Fluxes: Updates and Verification for the COARE Algorithm. *J Clim* **16**, 571–591 (2003).

5. Chen, F. & Dudhia, J. Coupling an Advanced Land Surface–Hydrology Model with the Penn State–NCAR MM5 Modeling System. Part I: Model Implementation and Sensitivity. *Mon Weather Rev* **129**, 569–585 (2001).

6. Schwalm, C. R., Glendon, S. & Duffy, P. B. RCP8.5 tracks cumulative CO2 emissions. *Proc Natl Acad Sci U S A* **117**, 19656–19657 (2020).

7. Jerez, S. *et al.* Impact of evolving greenhouse gas forcing on the warming signal in regional climate model experiments. *Nature Communications 2018 9:1* **9**, 1–7 (2018).

8. Giorgi, F., Jones, C. & Asrar, G. Addressing climate information needs at the regional level: the CORDEX framework. *... Organization (WMO) Bulletin* **58**, (2009).

9. Feron, S. *et al.* Observations and Projections of Heat Waves in South America. *Sci Rep* **9**, 8173 (2019).

10. Penalba, O. C. & Rivera, J. A. Future Changes in Drought Characteristics over Southern South America Projected by a CMIP5 Multi-Model Ensemble. *Am J Clim Change* **2**, 3 (2013).

11. Yin, L., Fu, R., Shevliakova, E. & Dickinson, R. E. How well can CMIP5 simulate precipitation and its controlling processes over tropical South America? *Clim Dyn* **41**, 3127–3143 (2013).

12. Palomino-Lemus, R., Córdoba-Machado, S., Gámiz-Fortis, S. R., Castro-Díez, Y. & Esteban-Parra, M. J. Summer precipitation projections over northwestern South America from CMIP5 models. *Glob Planet Change* **131**, 11–23 (2015).

13. Knist, S., Goergen, K. & Simmer, C. Evaluation and projected changes of precipitation statistics in convection-permitting WRF climate simulations over Central Europe. *Clim Dyn* **55**, 325–341 (2018).

14. Solman, S. A. & Blázquez, J. Multiscale precipitation variability over South America: Analysis of the added value of CORDEX RCM simulations. *Clim Dyn* **53**, 1547–1565 (2019).

15. Fonseca, D., Carvalho, M. J., Marta-Almeida, M., Melo-Gonçalves, P. & Rocha, A. Recent trends of extreme temperature indices for the Iberian Peninsula. *Physics and Chemistry of the Earth* **94**, 66–76 (2016).

16. Marta-Almeida, M., Teixeira, J. C., Carvalho, M. J., Melo-Gonçalves, P. & Rocha, A. M. High resolution WRF climatic simulations for the Iberian Peninsula: Model validation. *Physics and Chemistry of the Earth* **94**, 94–105 (2016).

17. Koutroulis, A. G., Grillakis, M. G., Tsanis, I. K. & Papadimitriou, L. Evaluation of precipitation and temperature simulation performance of the CMIP3 and CMIP5 historical experiments. *Clim Dyn* **47**, 1881–1898 (2016).

18. Akinsanola, A. A. & Zhou, W. Projection of West African summer monsoon rainfall in dynamically downscaled CMIP5 models. *Clim Dyn* **53**, 81–95 (2019).

19. Perkins, S. E., Pitman, A. J., Holbrook, N. J. & McAneney, J. Evaluation of the AR4 Climate Models' Simulated Daily Maximum Temperature, Minimum Temperature, and Precipitation over Australia Using Probability Density Functions. *J Clim* **20**, 4356–4376 (2007).